Global Normal-Mode Rossby Waves Observed in Stratospheric Ozone Data

WILLIAM J. RANDEL

National Center for Atmospheric Research, Boulder, Colorado*

(Manuscript received 20 November 1991, in final form 20 April 1992)

ABSTRACT

Westward-propagating Rossby normal-mode planetary waves are documented in stratospheric ozone data using Solar Backscatter Ultraviolet (SBUV) satellite measurements. These modes are evidenced by enhanced spectral power and near-global coherence for westward-traveling zonal wave 1 oscillations with periods of 5–10 days. The ozone waves have maxima in high latitudes of the middle stratosphere (due to transport) and over midlatitudes in the upper stratosphere (due to photochemistry). These modes are nearly continuous throughout the eight years of SBUV observations, with maximum global coherence during the equinoxes. The upper-stratospheric waves are symmetric (in phase) between hemispheres, even for modes previously identified as antisymmetric in geopotential height. This behavior is due to differing wave vertical structure in each hemisphere: the planetary *temperature* waves are nearly in phase in the upper stratosphere, even thogh the height waves are out of phase. The observed ozone waves are furthermore compared to calculations based on linear wave transport and photochemistry, incorporating derived wind and temperature fields. Good agreement is found, showing that normal modes provide an idealized context to study the linear wave behavior of trace constituents in the real atmosphere.

1. Introduction

Normal-mode Rossby waves are westward-propagating planetary waves, which are the free or resonant oscillations of the atmosphere. Their basic characteristics are governed by the resonant properties of the atmosphere, rather than by the details of any forcing mechanisms. The fundamental signatures of these modes are 1) planetary-scale horizontal structures, 2) regular westward propagation at (nearly) discrete frequencies, with typical periods of 5–20 days, and 3) small vertical phase tilts with height (see the review in Madden 1979). Theoretical predictions of normal-mode frequencies and spatial structures have been made using models with varying levels of sophistication (e.g., Kasahara 1980; Schoeberl and Clark 1980); detailed calculations for realistic solstice and equinox background flows are presented in Salby (1981). Numerous studies have identified normal-mode structures in observed (and modeled) atmospheric data; the identification as normal mode is usually based on 1) enhanced spectral power and global coherence for westward-propagating planetary waves near the appropriate normal-mode frequencies, and 2) horizontal and vertical structures consistent with theoretically predicted behavior. Normal modes have been observed in tropospheric geopotential height and wind data by Eliassen and Machenhauer (1965), Lindzen et al. (1984), and Ahlquist (1985). Stratospheric temperature and geopotential data derived from satellites have also shown conclusive evidence of normal modes (Rodgers 1976; Hirota and Hirooka 1984; Hirooka and Hirota 1985, 1989; Venne 1989). In this paper evidence is presented for regularly occurring normal-mode oscillations in satellite-derived measurements of the stratospheric ozone field.

The traveling ozone waves discussed here are not unanticipated in light of prior observations of stratospheric normal-mode height and temperature waves. In the lower stratosphere ozone acts as a material tracer and is advected in a wavelike manner by propagating waves, while in the upper stratosphere ozone is photochemically controlled and mirrors the temperature perturbations associated with traveling waves. Space–time spectral analyses of the global ozone data provided by the Solar Backscatter Ultraviolet (SBUV) satellite measurements show coherent traveling waves with global structures signifying normal modes. In this work the spatial and temporal characteristics of these modes are analyzed. Eight years of SBUV data show near-continuous presence of such modes with periods of 5–10 days; these data show a clear seasonality in global coherence, with maxima during the equinoxes. The ozone waves show relative maxima in the middle and upper stratosphere, due to transport and photochemical effects, respectively. An intriguing result is that the ozone waves in the upper stratosphere are found to be

* The National Center for Atmospheric Research is sponsored by the National Science Foundation.

Corresponding author address: Dr. William J. Randel, NCAR, P.O. Box 3000, Boulder, CO 80307-3000.

in phase between hemispheres, even for modes that have been previously identified as antisymmetric in geopotential height (in particular the 8–10-day zonal wave 1 mode).

This behavior is explored for several cases in detail by combined analyses with global geopotential height and temperature data. Results show that, due to differing wave vertical structures, the *temperature* waves in the upper stratosphere are in phase between hemispheres even though the heights are out of phase. Differences in vertical structure are likely due to differential wave attenuation in the background mean flows of the respective hemispheres. Because ozone responds primarily to temperature in the upper stratosphere, it too shows an in-phase structure. The ozone waves observed by SBUV are compared with calculations using a simple model of linear wave transport and photochemistry, incorporating winds and temperatures derived from observed data. Overall good agreement is found, demonstrating the accuracy of 1) the SBUV measurements (at least for the space and time scales analyzed here), 2) the derived perturbation meridional and vertical velocities, and 3) the model photochemical parameters used here. Overall, the normal modes provide an idealized context to study linear wave transport and photochemistry in the real atmosphere.

2. Data and analyses

The global ozone data analyzed here are based on profile measurements obtained from the SBUV instrument, which flew on the *Nimbus 7* spacecraft from late 1978 to early 1987. The ozone trends panel report (WMO 1991) discusses the information content of SBUV data, concluding that it should be capable of resolving the ozone profile from 16 to 0.5 mb (approximately 28 to 56 km), with a vertical resolution near 8–10 km. The data used here are mixing ratios at pressure levels 30, 20, 10, 7, 5, 3, 2, 1, 0.5, and 0.3 mb, which is oversampled in the vertical. The data at each pressure level were horizontally mapped using a Kalman filter, giving an estimate of the zonal mean and zonal waves 1–6 on a 4° latitude grid. Missing days' data are interpolated by the Kalman algorithm. We avoid the absence of data during polar night by focusing on latitudes 60°N–60°S.

In order to highlight wave structures throughout the middle and upper stratosphere, we analyze wave components of the ozone field normalized by the background zonal means, that is, $(\mu'/\bar{\mu})$. This normalization is discussed in Randel and Gille (1991), section 2b. Analyses of the normalized wave amplitudes also alleviate the long-term drifts apparent in the SBUV data, as discussed in Fleig et al. (1986) and WMO (1991).

Temperature and geopotential height data used here are operational stratospheric analyses covering 70–1 mb, produced at the National Meteorological Center/Climate Analyses Center (NMC/CAC). Overall, these data have similar space–time sampling as the SBUV data, with somewhat lower vertical resolution. The two datasets overlap for the 30-, 10-, 5-, 2-, and 1-mb pressure levels, and only these levels are used in cross-spectral calculations.

The global normal modes studied here are distinctive in that they exhibit strong global coherence, sharply peaked in zonal wavenumber and frequency, prompting the use of space–time cross-spectral analyses. We use the standard formulation given by Hayashi (1982) for eastward–westward cross-spectral calculations. All calculations use 120-day time series, and hence the frequency resolution is $\Delta\omega = (2\pi/120 \text{ days})$. We use direct Fourier transforms in time, and smooth the resulting spectral estimates with a normalized Gaussian-shaped filter of the form

$$W(\omega - \omega_0) = e^{-[(\omega-\omega_0)/N\Delta\omega]^2}. \quad (1)$$

Power spectra use (1) with $N = 2$, and cross spectra use (1) with $N = 3$ (a wider window is used to give greater statistical stability). The appropriate number of degrees of freedom is estimated from the power spectra using the equation in Blackman and Tukey (1958, p. 24); this gives a value of order 5 for the spectra here. The resulting 95% and 99% confidence levels for the coherence squared spectra (hereafter called simply coherence) are near 0.53 and 0.68, respectively.

3. Results

a. *Character of the global modes*

Statistical signatures of Rossby normal modes are seen in traveling wave power spectra as a concentration of power centered near the appropriate westward-propagating frequency bands, together with near-global statistical coherence (e.g., Hirota and Hirooka 1984; the horizontal and vertical structures of the modes are also fundamentally characteristic). Figure 1 shows power and coherence spectra for zonal wave 1 normalized ozone at the 1-mb level, calculated from data over April–July 1983. This time period is chosen because the waves exhibit relatively strong global coherence, as calculated and discussed in section 3b. The lower panel in Fig. 1 shows coherence at all latitudes with respect to a reference at 40°S. There is a near-global pattern of significant coherence for westward-moving waves with periods near 8–10 days (for simplicity this is referenced as a 9-day wave), and a weak secondary maximum near period 5 days. In contrast, eastward-moving waves are coherent only over high southern latitudes. The power spectra in Fig. 1 show distinct maxima centered near 40° in each hemisphere for the westward-moving 9-day wave.

As seen in Fig. 1 and in power spectra of other stratospheric variables (for example, geopotential height analyses of Hirota and Hirooka 1984), the spectral power associated with normal modes is not typi-

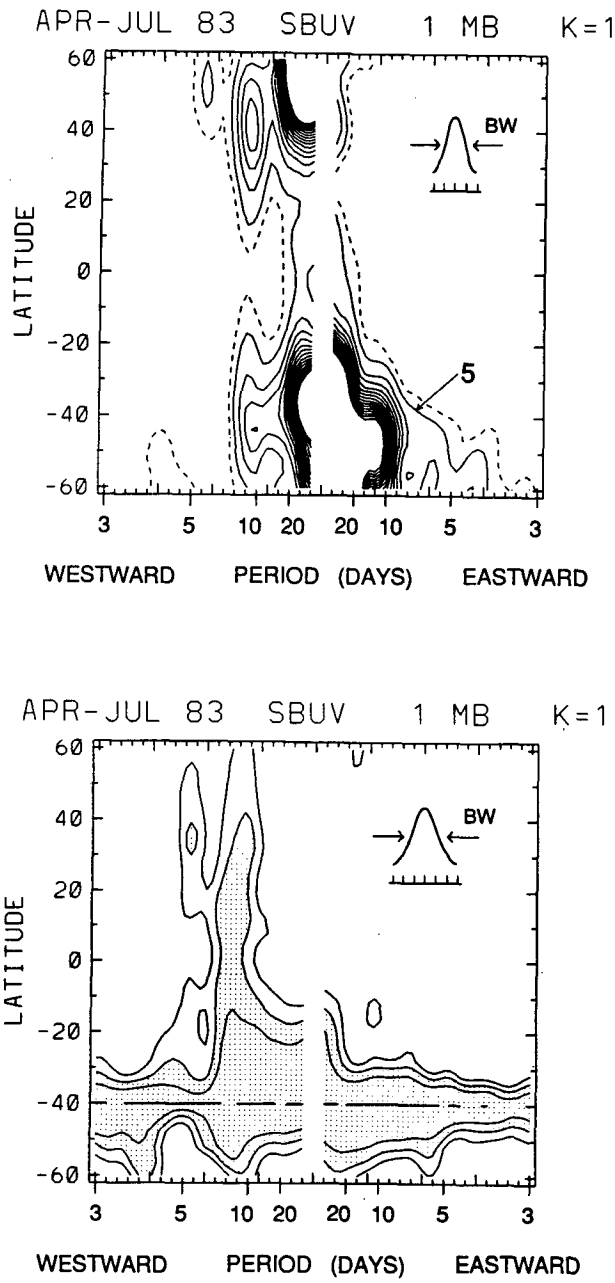

FIG. 1. (top) Power spectrum versus latitude of normalized zonal wave 1 ozone fluctuations at 1 mb for the period April–July 1983. Contour interval is $5 \times 10^{-6}\ \Delta\omega^{-1}$, and the dashed line is one-half the lowest contour. (bottom) Coherence squared spectrum for the same data, with respect to a reference latitude of 40°S. Contour levels are 0.4, 0.6, and 0.8, with values above 0.6 shaded. For these calculations the 95% confidence level is near 0.53. Spectral bandwidths (BW) for both calculations are shown.

cally a large fraction of the overall wave variance. In other words, normal modes are relatively small amplitude in long time averages. For short time intervals the modal amplitudes may become large, however, such that the entire wave field evolves with the space–time characteristics of a normal mode; such a case was analyzed by Madden and Labitzke (1980). Figure 2 shows such an example from the ozone observations during the time period analyzed in Fig. 1. Here the normalized ozone fields at 1 mb are shown during several days in July 1983; note that no space or time filtering has been applied to the data in Fig. 2, only the zonal means have been removed. A very clear westward-propagating zonal wave 1 pattern is seen in both hemispheres in Fig. 2, in phase between the Northern Hemisphere (NH) and Southern Hemisphere (SH). The NH wave amplitude is much smaller than that in the SH for this time period, although the spectral signature (Fig. 1) suggests more equal NH–SH amplitudes over the period April–July.

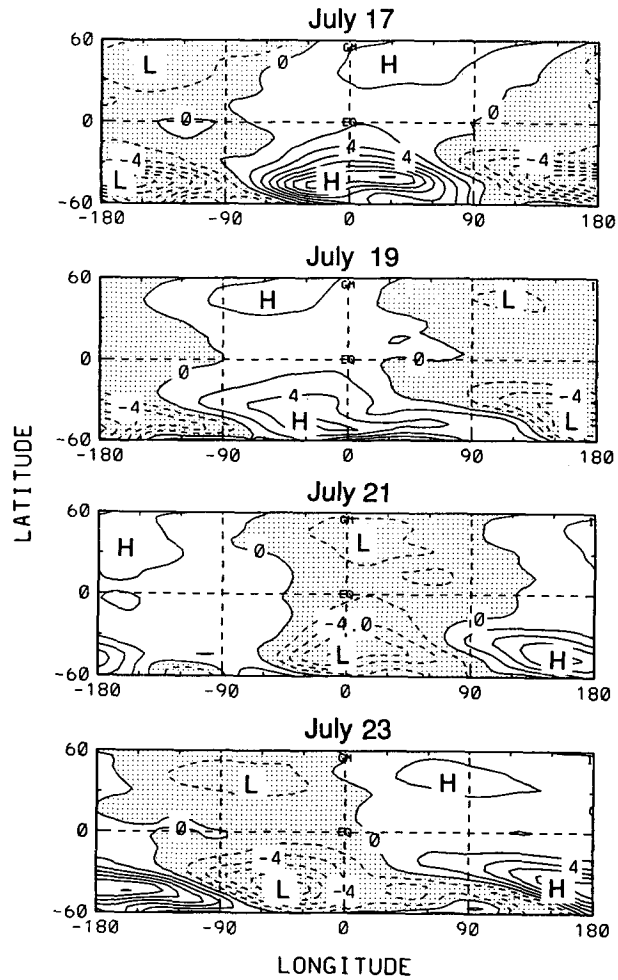

FIG. 2. Latitude–longitude plots of the normalized eddy ozone fields at 1 mb, for several days in July 1983 when a normal-mode Rossby wave was apparent. No space or time filtering has been applied to these data, only the zonal means have been removed. Note the global, westward-propagating zonal wave 1 feature with a period of order 9 days, with an in-phase meridional structure between hemispheres. Contour interval for the waves is 0.02 times the background zonal means.

A second example of a statistical normal-mode signature is shown in Fig. 3, using data over August–November 1986. Power spectral maxima and near-global coherence are observed for westward-moving waves with period near 7 days.

The height–latitude structures of the wave modes for these two time periods are shown in Fig. 4. Shown are the normalized wave amplitude and phase (with respect to 1 mb, 16°S), calculated for spectral bands centered on the appropriate frequencies. Wave amplitude is calculated as the square root of twice the summed spectral power. Normalized wave amplitudes show maxima in the midlatitude upper stratosphere centered near 1 mb, and in middle–high latitudes near 10–30 mb. Wave amplitudes are of order 0.01 times the background zonal means. The phase structures are in phase horizontally in the upper stratosphere (symmetric between hemispheres), with a weak westward phase tilt with height (corresponding to a vertical wavelength of order 60 km). Notably, each globally coherent event observed in the eight years of SBUV data, identified as discussed in the next section, exhibits this symmetric horizontal phase structure in the upper stratosphere. This is intriguing, because both theory (Salby 1981) and observations (Hirooka and Hirota 1985; Venne 1989) suggest that a wave 1 normal mode with period near 9 days (e.g., the April–July 1983 case in Fig. 4) should possess an antisymmetric or out of phase horizontal structure in geopotential height and temperature. This aspect will be analyzed further.

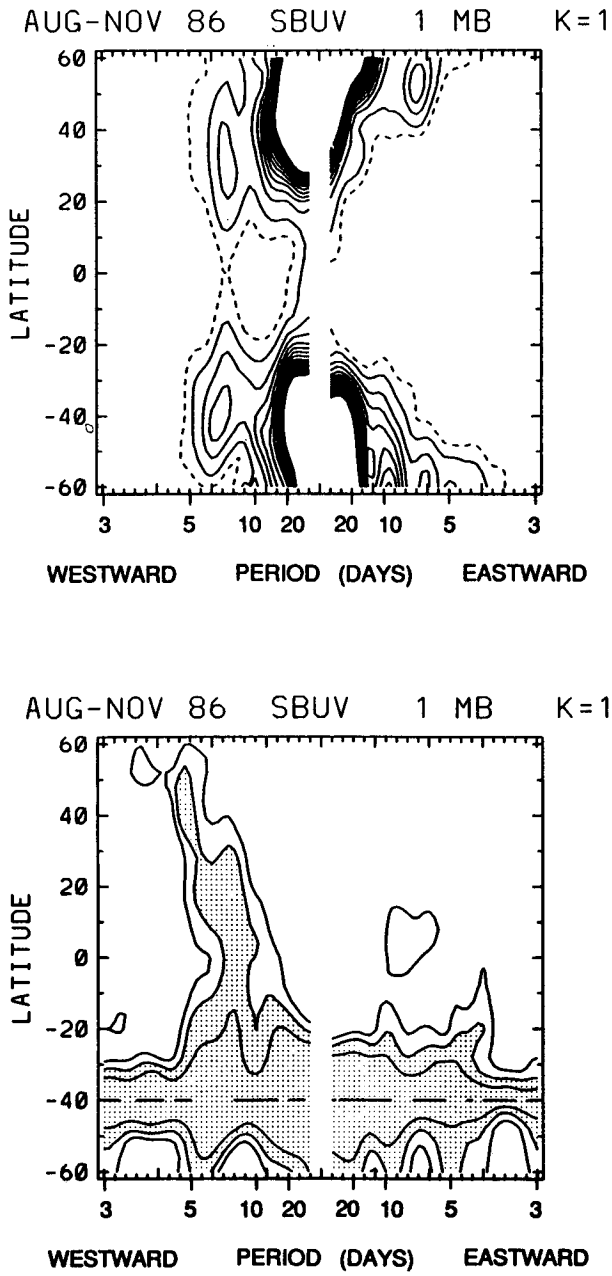

FIG. 3. Power and coherence spectra (as in Fig. 1) for zonal wave 1 at 1 mb, for data over August–November 1986.

b. Climatology

Figure 5 shows zonal wave 1 coherence squared between 32°N and 32°S for SBUV data covering the four years 1983–86; these spectra are calculated from overlapping 120-day time series centered on each month. This diagnostic illustrates the preferred frequencies or periods of global coherent modes that have sizable amplitudes near ±32°, along with identifying time periods when interhemispheric coherence is strongest. Figure 5 shows near-continuous occurrence of coherent modes for westward-propagating waves with periods in the range of 5–10 days. The exact central frequencies and bandwidths of coherence maxima vary from month to month; at times two separate frequencies are highlighted, such as near June 1983 (see Fig. 1) and July 1985.

Figure 6 shows the eight-year (1979–86) average-ensemble coherence spectra for zonal wave 1 between 32°N and 32°S. This shows a seasonal variation with maximum global coherence at periods of 5–8 days during the equinoxes (May–June and September–October), and a separate (weaker) maximum for 9–10-day periods during SH winter (June–July). The maximum in interhemispheric coherence during the equinoxes is likely related to the stratospheric background zonal wind structure: the calculations of Salby (1981) suggest that equinox conditions allow global westward modes, whereas they are attenuated or excluded in strong summer hemisphere easterlies. The minimum in global coherence during NH winter in Fig. 6 is an interesting result, possibly due to the summer hemisphere easterlies being substantially stronger at that time than during the corresponding period during SH winter [NMC climatology (Randel 1992) shows SH summer winds ≈ -50 m s^{-1} and NH summer winds ≈ -30 m s^{-1} at 1 mb].

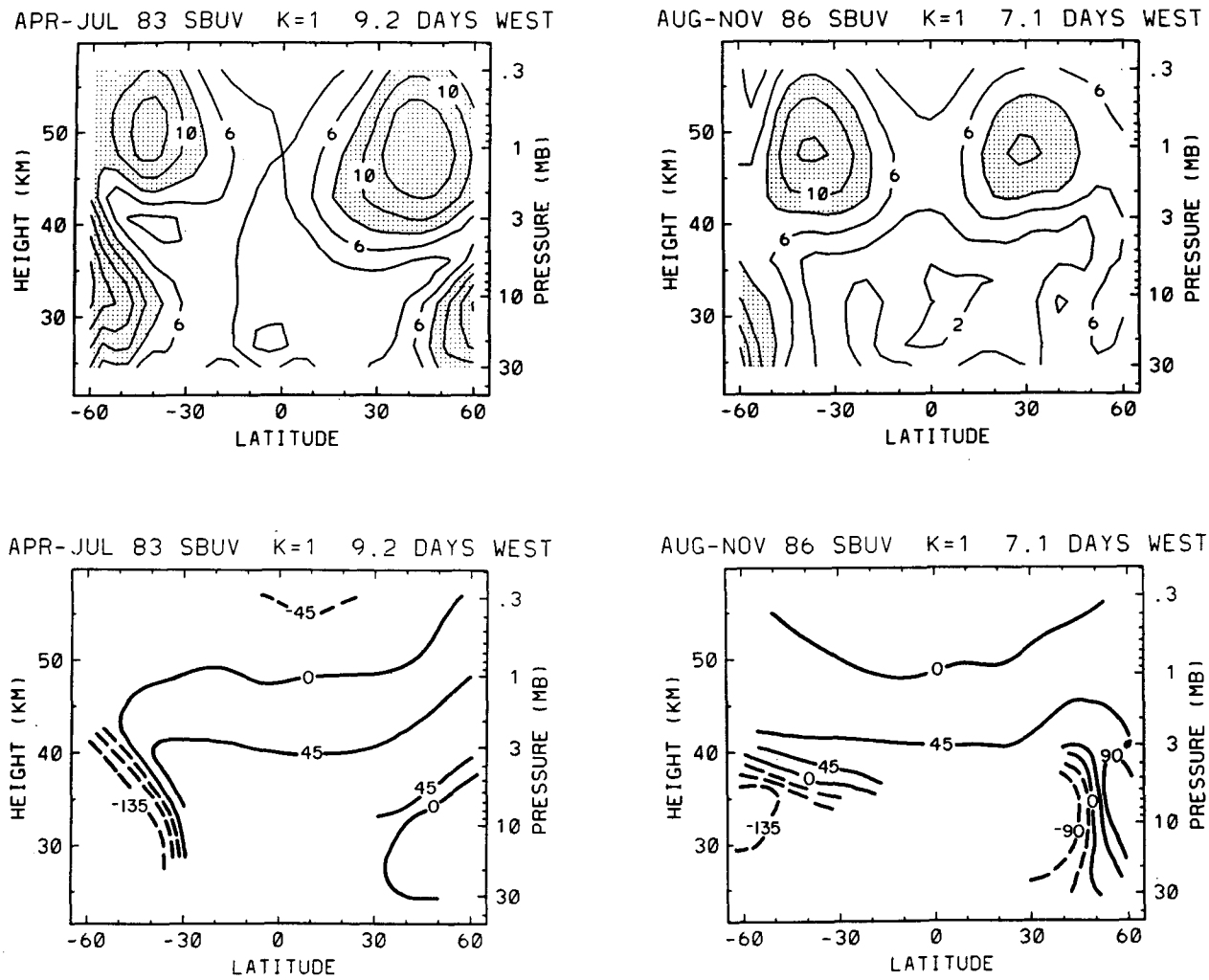

FIG. 4. Meridional cross sections of normalized ozone wave amplitude (top) and phase (bottom) for normal-mode Rossby waves identified from the spectra in Figs. 1 and 3. Contour interval for amplitude is 0.002 times the background zonal means. Phases (in degrees) are calculated with respect to 1 mb, 16°S, and only plotted where wave amplitudes are significant.

It is interesting to note the lack of global coherence in Figs. 5–6 for westward periods near 16 days, because such modes have been reported to be relatively strong in the NH winter stratosphere (Madden 1979; Madden and Labitzke 1980; Venne 1989). Figure 7 shows wave 1 power and coherence spectra at 0.5 mb during November 1978–February 1979, overlapping a time period of strong 16-day wave activity documented by Madden and Labitzke (1980). Power spectra in the NH are markedly red (maximum power at lowest frequencies), without a distinguishing westward maximum. The SH shows a maximum over 20°–40°S near westward periods of 7–9 days, and the coherence signature likewise highlights this frequency band. In contrast, periods near 16 days do not show evidence of global coherence. The lack of such a signature in these data is likely due to 1) the highly transient nature of the 16-day wave during this winter, and a resultant "washing out" in 120-day spectra, and 2) strong confinement of this relatively slower mode to the winter hemisphere, as suggested in the results of Salby (1981; see his Fig. 8).

c. *Comparison with temperature and geopotential data*

The observation of globally coherent, westward-propagating ozone waves is not surprising given the ubiquitous presence of Rossby normal modes in the stratosphere (see references in the Introduction). What is surprising is the symmetric latitudinal phase structure of the ozone waves in the upper stratosphere, for 8–10-day wave modes previously identified as antisymmetric. In this section wave structures in temperature

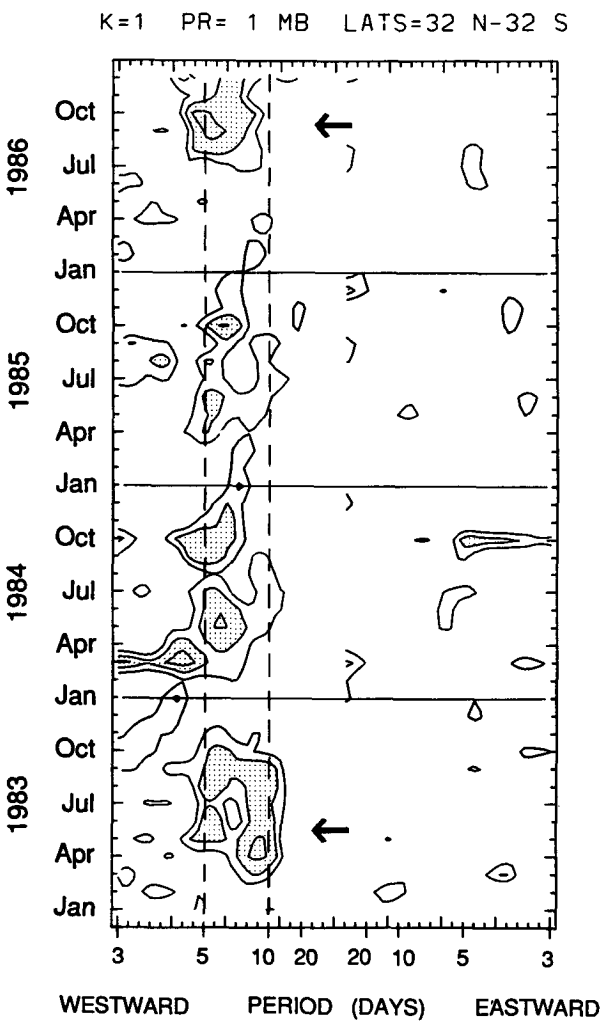

FIG. 5. Eastward–westward coherence squared spectra between latitudes 32°N and 32°S for zonal wave 1 ozone waves at 1 mb, SBUV data over 1983–86. Calculations are made using overlapping 120-day time series centered on each month. Contours are 0.4, 0.6, and 0.8, with values above 0.6 shaded. The 95% confidence level for these calculations is near 0.53. Note the near-continuous occurrence of strong coherence values for westward-propagating waves with periods 5–10 days. Time periods analyzed in Figs. 1–4 are indicated by the arrows.

and geopotential height data are analyzed in conjunction with the ozone data to explore this question.

Figure 8 shows zonal wave 1 power and coherence spectra at 1 mb for both ozone and temperature data, calculated over April–July 1981. Again, this time period is chosen as one of enhanced global coherence, based on examination of spectra as in Fig. 5. The ozone and temperature spectra in Fig. 8 are nearly identical, both highlighting a westward-moving wave near a 10-day period. The coherence spectra for both variables (not shown) is very similar to that seen in Fig. 1; additionally, the temperature data shows strong coherence for the 5-day mode, which is only hinted at in the ozone coherence spectra. This 5-day wave corresponds to the first symmetric wave 1 normal mode (e.g., Hirota and Hirooka 1984). Figure 9 shows the 1-mb geopotential power spectra for this time period, and the westward-moving 5- and 10-day modes are also observed; note that in all variables the 10-day wave has much larger amplitude than the 5-day wave. It is worth noting that this time period was also studied by Hirooka and Hirota (1985), who identify a 9.2-day westward-moving geopotential wave with antisymmetric latitudinal phase structure (see their Fig. 2).

Figure 10 shows meridional cross sections of amplitude and phase for the 10-day waves in ozone, temperature, and geopotential height; note that the phases are calculated for each variable separately and do not give information on phase differences between variables (these are discussed later). For reference, the zonal wind structure for this period is shown in Fig. 11. The geopotential wave has a factor of 2 larger amplitude in the SH and weak vertical phase tilt; the smaller NH maximum tilts slowly westward with height. The NH and SH maxima are approximately 135° out of phase. The variable phase structure seen in the geopotential height wave might suggest that more than one individual normal mode is present during this time period (M. Salby, personal communication). As a test of this idea, Fig. 12 shows geopotential height power spectra at 40°N and S, at 30 and 1 mb. Spectra at all four positions show a sharp peak centered near period 10 days (westward); the 40°N, 1-mb spectra also shows a second peak corresponding to the 5-day mode previously discussed, although a corresponding 5-day peak is not seen in the SH. The sharp spectral peaks centered

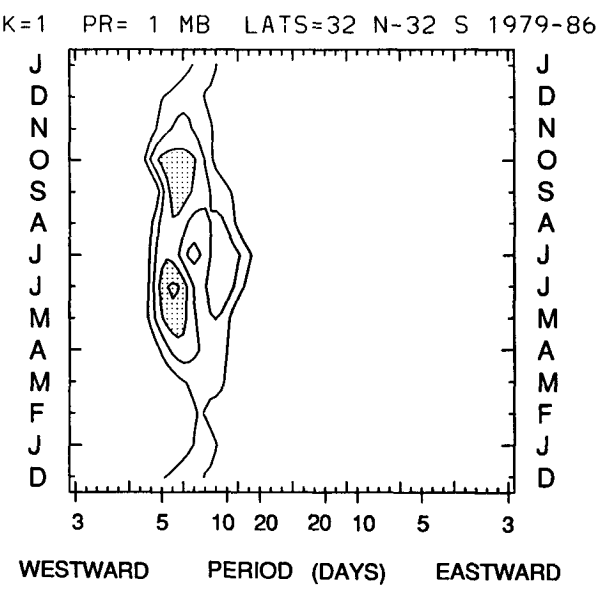

FIG. 6. Ensemble eight-year average coherence spectra for 1-mb zonal wave 1 ozone waves between 32°N and 32°S. Contours are 0.15, 0.25, · · · . The 95% confidence level is near 0.19.

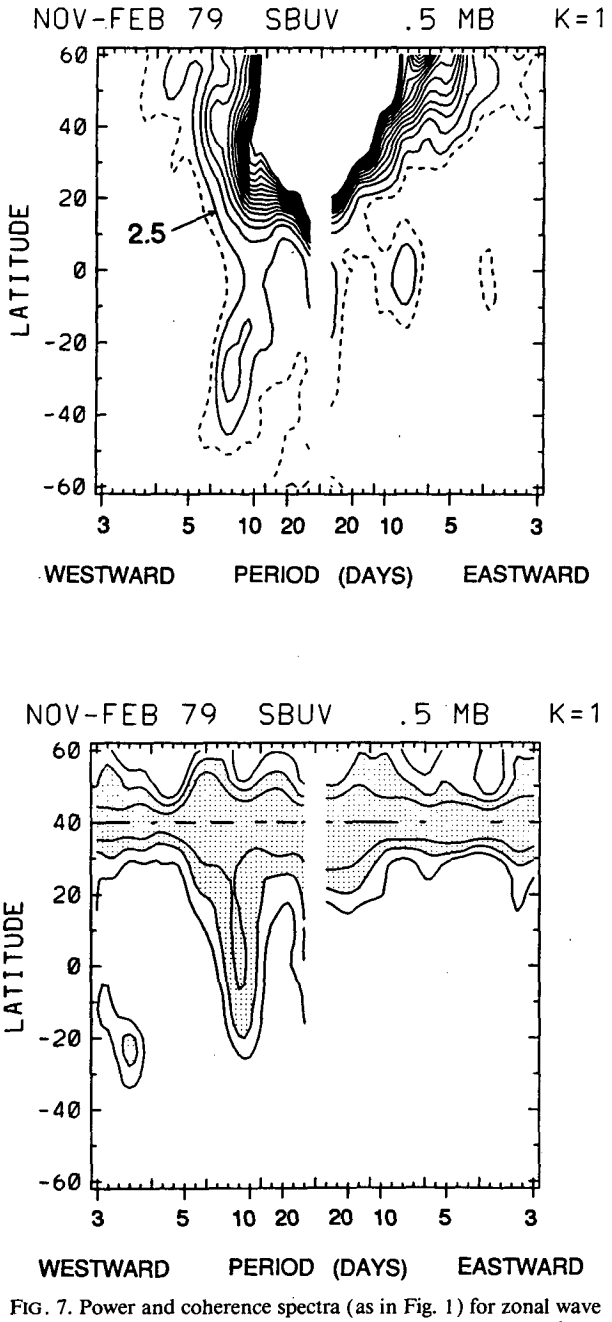

FIG. 7. Power and coherence spectra (as in Fig. 1) for zonal wave 1 at 0.5 mb, for data over November 1978–February 1979.

near the same frequency throughout the meridional plane demonstrate that the 10-day wave structure isolated in Fig. 10 corresponds to that for a single normal mode. As a note, the geopotential modal structure shown in Fig. 10 is substantially different from that calculated by Salby (1982) for either equinox or solstice backgrounds. This is not surprising, however, because the observed winds during this intermediate season (Fig. 11) are very different from the idealized winds used in those calculations.

The temperature wave structure in Fig. 10 shows less asymmetry in amplitude between hemispheres than the geopotential wave, with roughly a factor of 1.2–1.5 larger amplitude in the SH. The temperature wave tilts slowly westward with height in the SH, and more rapidly with height at high northern latitudes. Note that there is *not* a rapid horizontal phase shift between the 1-mb temperature maxima near 40°N and 40°S, and in fact, the temperature wave is nearly in phase latitudinally in the upper stratosphere. In the lower stratosphere (~30 mb) the temperature and geopotential waves are both approximately out of phase between 40°N and 40°S. Recall that the temperature and geopotential height waves are in hydrostatic balance (involving both amplitude and phase); the larger-amplitude, nearly barotropic SH geopotential wave and the smaller but stronger tilting NH wave are in balance with nearly equal-amplitude temperature waves. Furthermore, the temperature wave at 1 mb has a symmetric rather than antisymmetric latitudinal structure.

The normalized ozone wave in Fig. 10 shows the same overall amplitude and phase structure as those shown in Fig. 4, in particular in-phase horizontal structure in the upper stratosphere. The ozone wave structure in Fig. 10 also shows a relative maximum centered near 10 mb, 40°S in the SH, and one in the high-latitude NH over 10–30 mb. The 10–30-mb ozone waves are approximately 180° out of phase between hemispheres.

Meridional cross sections of coherence and phase between ozone and temperature waves are shown in Fig. 13. Significant coherence is found over the entire globe in the upper stratosphere (5–1 mb), and over 30°–60° in each hemisphere in the lower–middle stratosphere (30–10 mb). The ozone and temperature waves are out of phase in the upper stratosphere and in phase in the lower stratosphere. The phase transition region occurs at a higher altitude in the SH (near 40 km) than in the NH (near 35 km). In-phase ozone–temperature waves signify a transport-controlled region, whereas out-of-phase variations may be attributable to photochemistry or transport (e.g., Rood and Douglass 1985). Below, the separate contributions are explicitly calculated.

d. Comparison of observed and calculated ozone variations

In this section the observed normal-mode ozone oscillations are compared with those predicted by a model of linear wave transport and photochemistry. The waves in question here certainly satisfy a linear criterion (wave amplitudes of order 0.01 times background fields), and the waves' coherently propagating character invites a detailed comparison with linear wave theory. Good agreement is found between observations and theory, validating (among other things) the photochemical parameters and transport velocities used here.

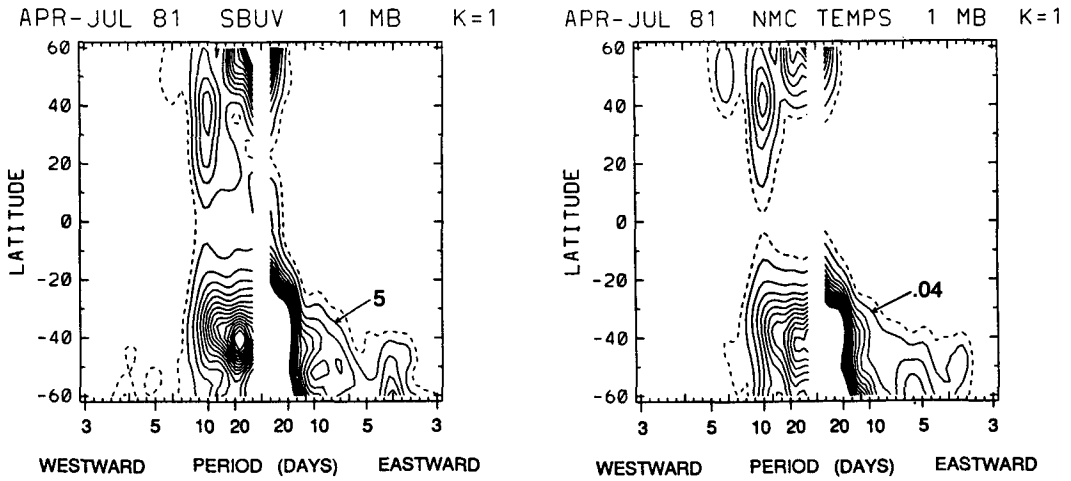

FIG. 8. Power spectra for normalized ozone (left) and temperature (right) data. Calculations are for zonal wave 1 at 1 mb, using data over April–July 1981. Ozone spectra contours as in Fig. 1, with temperature power contours of 0.04 $K^2\,\Delta\omega^{-1}$.

The calculated ozone variations are based on the linearized ozone continuity equation discussed in Hartmann and Garcia (1979) and Rood and Douglass (1985):

$$\left(\frac{\partial}{\partial t} + \bar{u}\frac{\partial}{\partial x}\right)\mu' + v'\bar{\mu}_y + w'\bar{\mu}_z = -\Gamma\mu' - \Theta T'. \quad (2)$$

Here μ' is the perturbation ozone mixing ratio, Γ and Θ ozone photochemical parameters, and other symbols have their usual meaning. The Γ and Θ values used here are based on the calculations in Stolarski and Douglass (1985), averaged for April–July background conditions, as provided by Anne Douglass (private communication). Normal-mode meridional winds (v') were calculated from the geopotential data via a balance scheme, and vertical winds (w') were calculated from the linearized thermodynamic equation:

$$\left(\frac{\partial}{\partial t} + \bar{u}\frac{\partial}{\partial x}\right)T' + v'\bar{T}_y + w'S = 0, \quad (3)$$

with

$$S = \frac{1}{H}\left(\frac{2}{7}\bar{T} + \frac{\partial \bar{T}}{\partial z}\right),$$

a background static stability parameter. Radiative damping is neglected in Eq. (3) because realistic radiative time scales in the stratosphere (of order 10 days) are much longer than the wave advective time scale (of order 1–2 days). Calculated meridional and vertical wind amplitudes for the normal mode are of order 1 m s^{-1} and 0.1 cm s^{-1}, respectively.

Because we are concerned with zonally propagating waves, we seek solutions to Eq. (2) of the form:

$$\mu'(x, t) = \mu s \cdot \sin k(x - ct) + \mu c \cdot \cos k(x - ct), \quad (4)$$

and likewise for other wave quantities v', w', and T'. Equation (2) may then be solved for the spectral coefficients μs and μc:

$$\mu s = (k^2(\bar{u} - c)^2 + \Gamma^2)^{-1} \times [\bar{\mu}_y(-k(\bar{u} - c)\cdot vc - \Gamma \cdot vs) + \bar{\mu}_z(-k(\bar{u} - c)\cdot wc - \Gamma \cdot ws) + \Theta(-k(\bar{u} - c)\cdot Tc - \Gamma \cdot Ts)] \quad (5a)$$

$$\mu c = (k^2(\bar{u} - c)^2 + \Gamma^2)^{-1} \cdot [\bar{\mu}_y(k(\bar{u} - c)\cdot vs - \Gamma \cdot vc) + \bar{\mu}_z(k(\bar{u} - c)\cdot ws - \Gamma \cdot wc) + \Theta(k(\bar{u} - c)\cdot Ts - \Gamma \cdot Tc)]. \quad (5b)$$

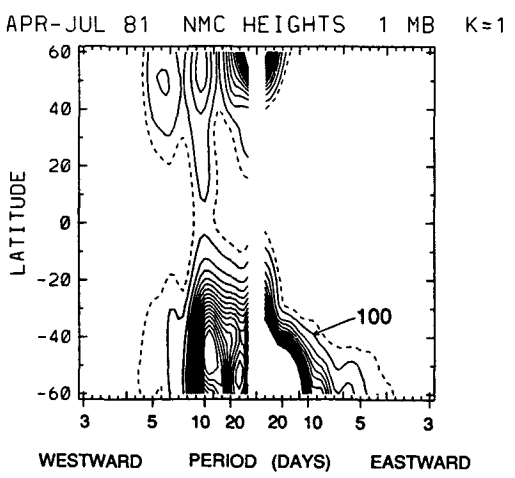

FIG. 9. Power spectra for 1-mb wave 1 geopotential height data, for the same time period as in Fig. 8. Contours are 100 $gpm^2 \cdot \Delta\omega^{-1}$.

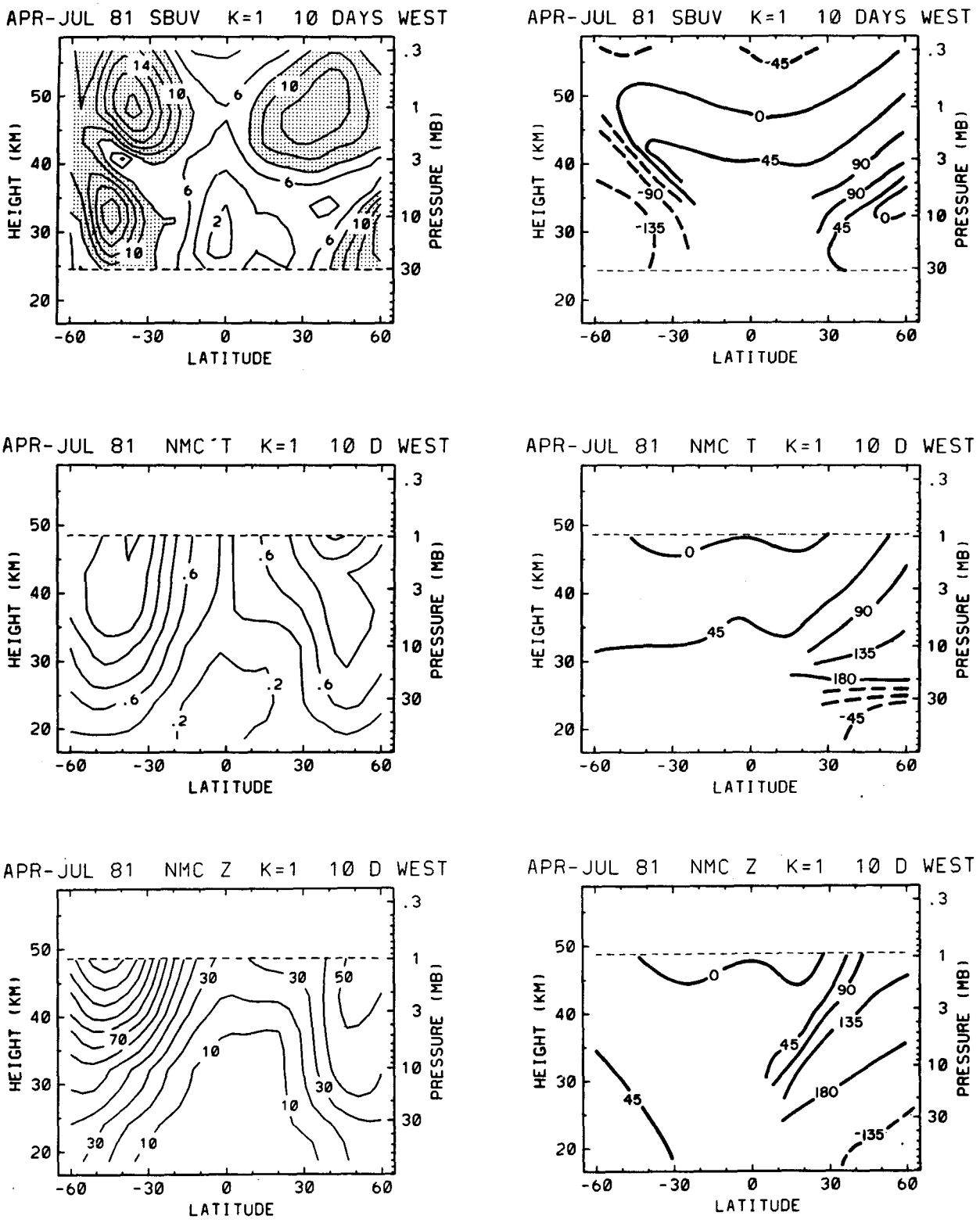

FIG. 10. Meridional cross sections of wave amplitudes and phases for the 10-day westward-propagating Rossby normal mode during April–July 1981, as identified in Figs. 8–9. Shown are normalized ozone (top, amplitude contours of 0.002), temperature (middle, K), and geopotential height (bottom, gpm). Phases are in degrees, calculated with respect to 16°S, 1 mb for each variable. Note that the temperature and height data only extend to 1 mb.

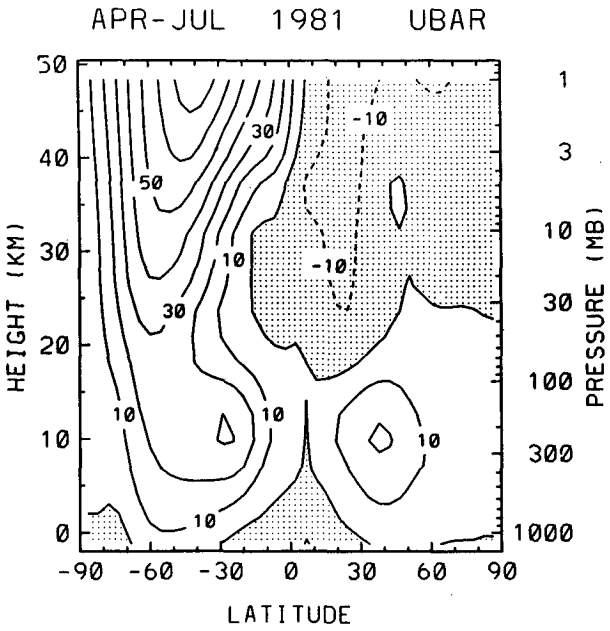

FIG. 11. Zonal-mean zonal wind during April–July 1981. Contours are 10 m s^{-1}.

Note that these equations are for unnormalized ozone variations, and are easily normalized by division by $\bar{\mu}$.

Figure 14 shows the normalized ozone wave amplitude $(\mu s^2 + \mu c^2)^{1/2}/\bar{\mu}$, calculated from Eq. (5), using wind and temperature fields filtered to retain only the westward-propagating 10-day wave. The corresponding observed amplitude is shown in Fig. 10; note the calculated amplitude can only be derived to 1 mb. There is good agreement in both spatial pattern and magnitude between observed and calculated ozone waves; note that the SH maximum near 10 mb over 30°–50°S and the NH maximum polewards of 40°N over 10–30 mb are seen in both sections. The phase of the calculated wave (not shown) is nearly identical to that observed (Fig. 10).

Figures 15–16 show time series of the observed zonal wave 1 coefficient of normalized ozone, and that calculated by Eq. (5b), at several latitude–height locations (Fig. 15 is for the SH and Fig. 16 for the NH—the positions are noted in Fig. 14). These time series were calculated by filtering the data to retain only westward-propagating waves with periods in the band 8.0–13.3 days, using the equations in appendix B of Ziemke and Stanford (1990); this bandwidth is indicated in Fig. 12. Also shown in the right-hand panels of Figs. 15–16 are contributions from the separate terms within the brackets on the right-hand side of Eq. (5b); these terms sum to the total calculated ozone (dashed lines) shown in the left-hand panels. The contributions are separated as 1) terms with only $\bar{\mu}_y$, $\bar{\mu}_z$, and $k(\bar{u} - c)$ (horizontal and vertical transports), 2) a term with only Θ and Γ (photochemical), and 3) terms with a combination of 1) and 2) (called "mixed"). This separation allows evaluation of the important mechanism(s) controlling ozone change at each position.

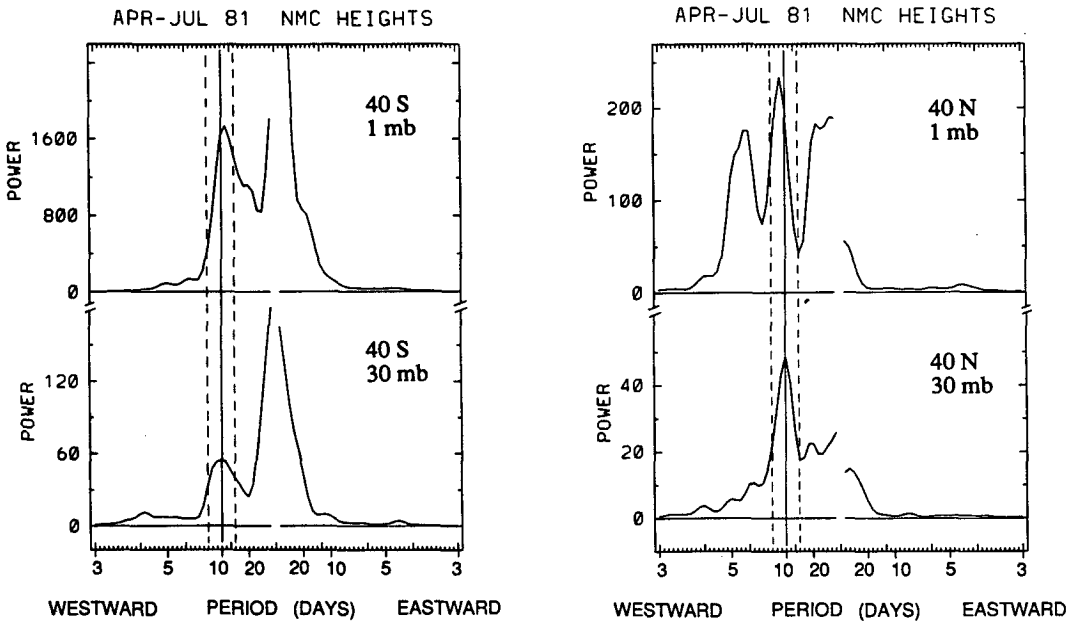

FIG. 12. April–July 1981 power spectra for zonal wave one geopotential heights at 40°S (left) and 40°N (right), for pressure levels 1 mb (top) and 30 mb (bottom). Note the peak corresponding to a westward-propagating wave with period centered near 10.0 days at each location. The spectral band of periods 8.0–13.3 days is also indicated, as used to isolate the structure of this mode in Fig. 10.

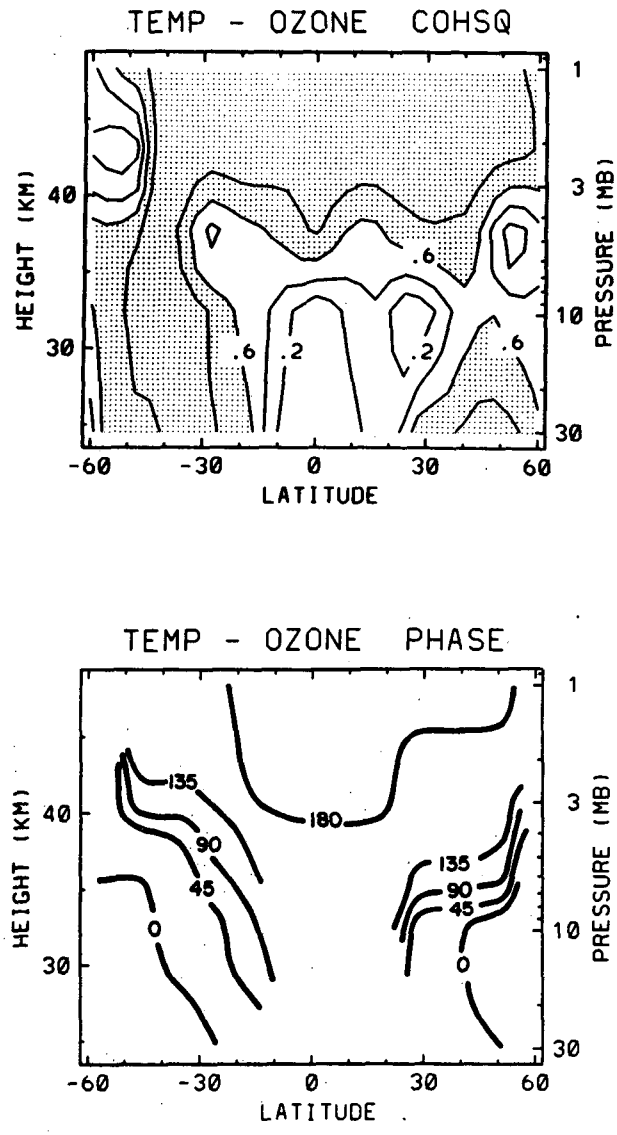

FIG. 13. Meridional cross sections of coherence squared and phase between ozone and temperature waves for the 10-day Rossby normal mode during April–July 1981.

First of all, the observed and calculated ozone variations show overall good agreement in both amplitude and phase, although calculated values are underestimates at some positions (30 mb, 40°S and 2 mb, 40°N). This agreement is most amazing when it is recalled that the observed and calculated data are derived from completely different satellite measurements (SBUV ozone versus NMC temperature data). Note the modulation of wave activity throughout the 120 days of analyses, and the overall out-of-phase behavior between the upper and lower stratosphere. Vertical transport is dominant at 30 mb in both hemispheres, although the calculated values are only about half those observed in the SH. The 10-mb data show relative maxima in wave amplitude (Fig. 14), and here observed and calculated ozone values show exceptional agreement (Figs. 15–16). Horizontal transports dominate at this level, although "mixed" terms are also large in the NH, showing that photochemistry cannot be neglected. The relative importance of horizontal transport at 10 mb versus vertical transport at 30 mb is due primarily to the respective structures of $\bar{\mu}_y$ and $\bar{\mu}_z$. As indicated in Fig. 17, $\bar{\mu}_z$ is small near the zonal-mean ozone maximum at 10 mb, but $\bar{\mu}_y$ maximizes near this level. Furthermore, vertical velocities are minutely small for this nearly barotropic normal mode: (w'/v') ratios are $\sim 10^{-3}$ here versus 10^{-2} for more strongly baroclinic waves in the lower stratosphere. The dominance of horizontal transport for the normal modes is why they have the typical signature of maxima in middle–high latitudes near 10 mb (cf. Figs. 4 and 10).

Photochemical terms are completely dominant in the NH at 2 and 1 mb (Fig. 16); calculated values at 1 mb agree better with observations than those at 2 mb. In the SH upper stratosphere, transport and "mixed" terms are also important, particularly at 2 mb. Note that all the separate transport and photochemistry terms are in phase in the SH upper stratosphere. The relative difference between the hemispheres in the importance of upper-stratospheric transport processes is due mainly to the background zonal wind structure (see Fig. 11). In the SH during this time period, $\bar{u} \sim 70$ m s^{-1} and the advective time scale $[k(\bar{u} - c)]^{-1}$ is $\sim$0.6 day, while in the NH, $\bar{u} \sim 0$ m s^{-1} and $[k(\bar{u} - c)]^{-1} \sim 2$ days. Comparison with the photochemical relaxation time scale of $\sim$0.3 day shows

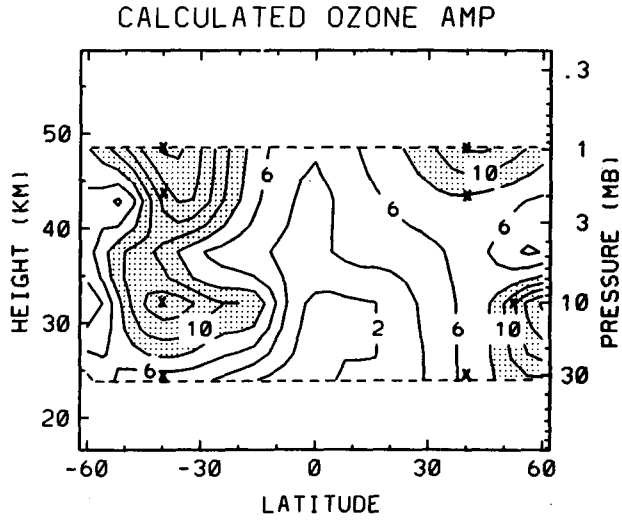

FIG. 14. Meridional cross section of normalized ozone normal-mode wave amplitude calculated from Eq. (5), using the analyzed wind and temperature data discussed in text. Compare with the observed wave amplitude structure shown in Fig. 10. The ×'s denote locations for the time series shown in Figs. 15–16.

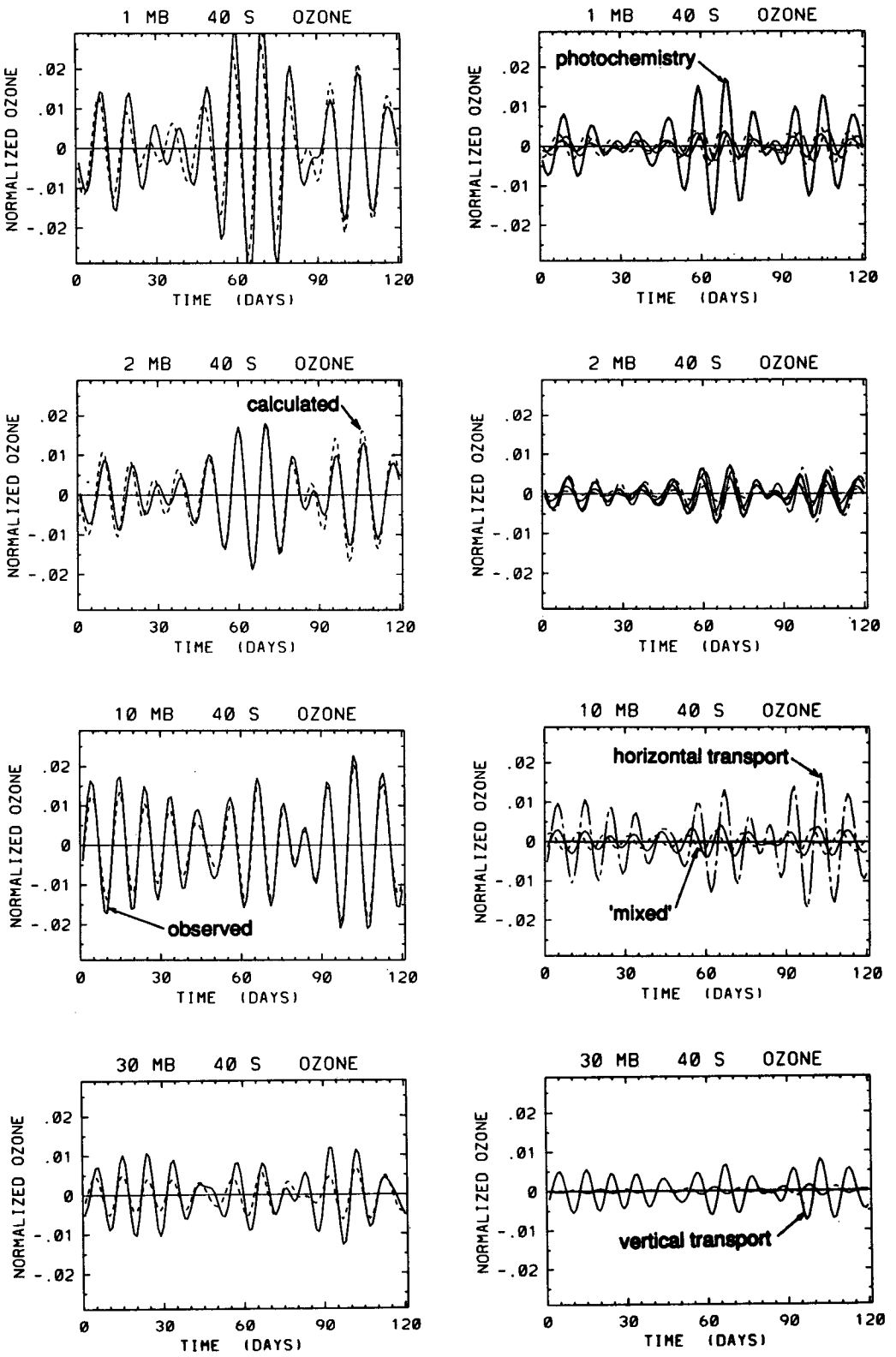

FIG. 15. Left panels compare observed wave 1 ozone cosine coefficient time series (solid lines) with those calculated using Eq. (5b) (dashed lines), at several SH locations (noted in Fig. 14). The time period covered is April–July 1981. Data have been filtered to retain only westward-propagating components with periods of 8.0–13.3 days. Right panels show separate contributions to the calculated values, separated as discussed in text; note that the individual curves in the right-hand panels sum to the dashed lines in the left panels.

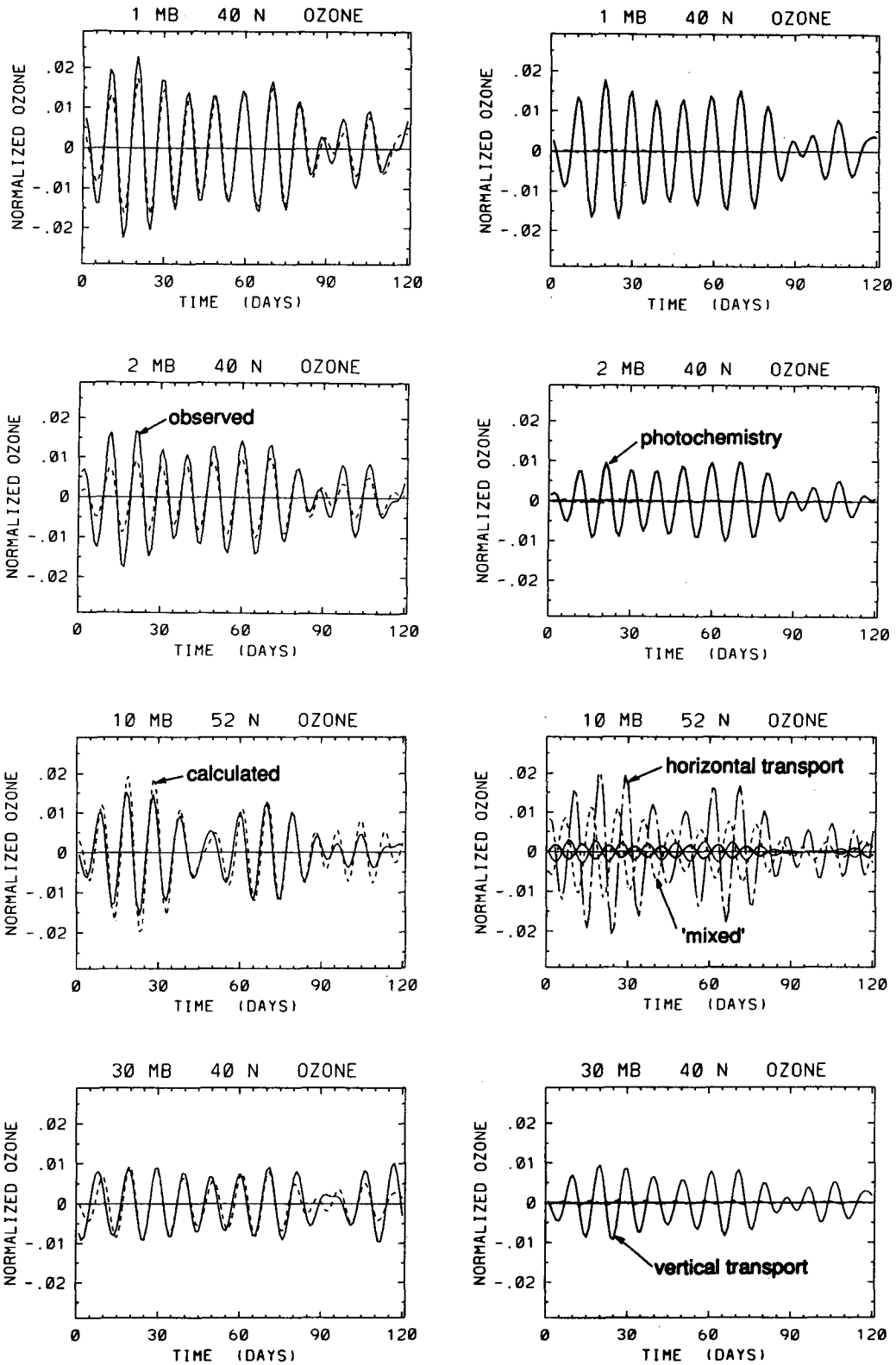

FIG. 16. As in Fig. 15 but for the NH positions noted in Fig. 14.

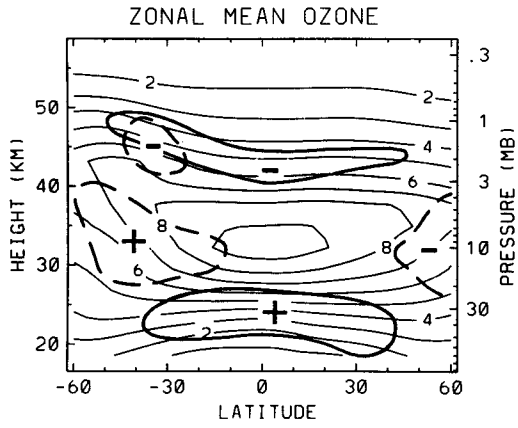

FIG. 17. Meridional cross section of zonal-mean ozone ($\bar{\mu}$) for April–July 1981 (light lines, contour interval of 1 ppmv). Heavy lines denote regions of largest $\bar{\mu}_z$ (solid) and $\bar{\mu}_y$ (dashed).

why transport is more important in the SH than in the NH. This also explains why the transition region is higher in the SH than in the NH (see Fig. 13).

4. Summary

Space–time spectral analyses have been used to identify global normal-mode Rossby wave signatures in the stratospheric ozone field. Here 5–10-day westward-propagating zonal wave 1 modes are observed throughout the eight years of SBUV measurements; globally coherent modes are most evident during equinox backgrounds. Analyses for zonal wave 2 did not show such globally coherent features. The ozone waves show relative maxima in the middle and upper stratosphere in middle and high latitudes. The middle stratosphere maxima are due mainly to horizontal transport; vertical transports (which maximize near 30–50 mb) are relatively small due to the minute vertical velocities associated with the normal modes. Upper-stratospheric ozone maxima are mainly photochemical in origin, responding to the normal-mode temperature perturbations (although transport is not necessarily negligible). Horizontal structure of the ozone waves in the upper stratosphere is observed to be symmetric between hemispheres for all cases and frequencies examined, even for the 8–10-day wave 1 mode previously identified as antisymmetric in geopotential height. For this latter case, examination of wave structures here demonstrated that although the geopotential height perturbations are antisymmetric, the temperature waves are symmetric in the upper stratosphere, and hence the ozone (which responds primarily to the temperature) is also. Similar height–temperature wave structures were found for other individual cases examined, so that this appears to be a typical situation during equinoxes, when globally coherent modes are most prevalent in the upper stratosphere.

The global modes studied here occasionally exhibit large amplitudes in the summer hemisphere stratosphere, and may contribute substantially to the overall variance there (note the NH patterns in Fig. 2). Constituent oscillations associated with normal modes provide a mechanism for summer stratosphere variability that complements the mechanism proposed in Hess and Holton (1985). Transport oscillations will most readily be apparent in long-lived constituents with strong background meridional gradients in high latitudes, such as HNO_3, HCl, and HF.

Although the normal-mode ozone wave amplitudes are small (order 0.01 times background values) and contain small fractions of the overall wave variance, their sharp concentration in wavenumber-frequency space makes them useful as examples of linear waves in the real atmosphere. As such, they invite detailed comparisons with linear wave theory, and are useful for studying wave transport and photochemistry in an idealized context. The overall good agreement found here between observed and calculated ozone variations (Figs. 15–16) can be viewed as quality checks on 1) the SBUV observations, at least for the deep vertical structures and 10-day time scales analyzed here, 2) calculated perturbation winds v' and w', and 3) the photochemical parameters Θ and Γ. Similar studies of more complicated dynamical–photochemical interactions may be possible with future satellite observations of global constituent data.

Acknowledgments. The author thanks Anne Smith, Rolando Garcia, Larry Lyjak, Roland Madden, and Murry Salby for helpful reviews and discussions. The ozone data were provided by John Gille, and the horizontal mapping was implemented by Dan Packman. Marilena Stone expertly prepared the manuscript. This work was supported under NASA Grant W 16215.

REFERENCES

Ahlquist, J. E., 1985: Climatology of normal mode Rossby waves. *J. Atmos. Sci.*, **42**, 2059–2068.

Blackman, R. B., and J. W. Tukey, 1958: *The Measurement of Power Spectra.* Dover, 190 pp.

Eliasen, E., and B. Machenhauer, 1965: A study of the atmospheric planetary flow represented by spherical harmonics. *Tellus*, **17**, 220–238.

Fleig, A. J., P. K. Bhartia, and D. S. Silberstein, 1986: An assessment of the long-term drift in SBUV total ozone data, based on comparison with the Dobson network. *Geophys. Res. Lett.*, **13**, 1359–1362.

Hartmann, D. L., and R. R. Garcia, 1979: A mechanistic model of ozone transport by planetary waves in the stratosphere. *J. Atmos. Sci.*, **36**, 350–364.

Hayashi, Y., 1982: Space–time spectral analysis and its application to atmospheric waves. *J. Meteor. Soc. Japan*, **60**, 156–171.

Hess, P. G., and J. R. Holton, 1985: The origin of temporal variance in long-lined trace constituents in the summer stratosphere. *J. Atmos. Sci.*, **42**, 1455–1463.

Hirooka, T., and I. Hirota, 1985: Normal mode Rossby waves observed in the upper stratosphere. Part II: Second antisymmetric

and symmetric modes of zonal wave numbers 1 and 2. *J. Atmos. Sci.*, **42**, 536–548.

——, and ——, 1989: Further evidence of normal mode Rossby waves. *Pure Appl. Geophys.*, **130**, 277–289.

Hirota, I., and T. Hirooka, 1984: Normal mode Rossby waves observed in the upper stratosphere. Part I: First symmetric modes of zonal wave numbers 1 and 2. *J. Atmos. Sci.*, **41**, 1253–1267.

Kasahara, A., 1980: Effect of zonal flows on the free oscillations of a barotropic atmosphere. *J. Atmos. Sci.*, **37**, 917–929.

Lindzen, R. S., D. M. Straus, and B. Katz, 1984: An observational study of large-scale atmospheric Rossby waves during FGGE. *J. Atmos. Sci.*, **41**, 1320–1335.

Madden, R. A., 1979: Observations of large-scale traveling Rossby waves. *Rev. Geophys. Space Phys.*, **17**, 1935–1949.

——, and K. Labitzke, 1981: A free Rossby wave in the troposphere and stratosphere during January 1979. *J. Geophys. Res.*, **86**, 1247–1254.

Randel, W. J., 1992: Global Atmospheric Circulation Statistics, 1000–1 mb. NCAR Tech. Note TN-366+STR, 256 pp.

——, and J. C. Gille, 1991: Kelvin wave variability in the upper stratosphere observed in SBUV ozone data. *J. Atmos. Sci.*, **48**, 2336–2349.

Rodgers, C. D., 1976: Evidence for the five-day wave in the stratosphere. *J. Atmos. Sci.*, **33**, 710–711.

Rood, R. B., and A. R. Douglass, 1985: Interpretation of ozone temperature correlations 1. Theory. *J. Geophys. Res.*, **90**, 5733–5743.

Salby, M., 1981: Rossby normal modes in nonuniform background conditions. Part II: Equinox and solstice conditions. *J. Atmos. Sci.*, **38**, 1827–1840.

Schoeberl, M. R., and J. H. E. Clark, 1980: Resonant planetary waves in a spherical atmosphere. *J. Atmos. Sci.*, **37**, 20–28.

Stolarski, R. S., and A. R. Douglass, 1985: Parameterization of the photochemistry of stratospheric ozone including catalytic loss processes. *J. Geophys. Res.*, **90**, 10 709–10 718.

Venne, D. E., 1989: Normal-mode Rossby waves observed in the wave number 1–5 geopotential fields of the stratosphere and troposphere. *J. Atmos. Sci.*, **46**, 1042–1056.

World Meteorological Organization (WMO), 1991: Report of the International Ozone Trends Panel—1988, WMO Report No. 18, World Meteorological Organization, Geneva.

Ziemke, J. R., and J. L. Stanford, 1990: One-to-two month oscillations in the stratosphere during Southern winter. *J. Atmos. Sci.*, **47**, 1778–1793.